Hindawi
Mathematical Problems in Engineering
Volume 2018, Article ID 4012451, 12 pages
https://doi.org/10.1155/2018/4012451

Research Article

Numerical Analysis of Stress Fields and Crack Growths in the Floor Strata of Coal Seam for Longwall Mining

Lingzhi Sun,[1,2] Yunyue Xie,[1,2] and Hongtian Xiao [1,2]

[1] *College of Civil Engineering and Architecture, Shandong University of Science and Technology, China*
[2] *Shandong Key Lab of Civil Engineering Disaster Prevention & Mitigation, Qingdao 266510, China*

Correspondence should be addressed to Hongtian Xiao; xiaohongtian@tsinghua.org.cn

Received 22 March 2018; Accepted 31 July 2018; Published 15 August 2018

Academic Editor: Andras Szekrenyes

This paper predicts the possibility of water inrush from a confined aquifer under the action of mining activities and water pressure. The study uses numerical analyses to evaluate stress redistribution and crack growth which result from coal extraction operations. Two models are presented in this study. By simplifying the distribution of the disturbed vertical stress on the coal seam and floor around a working face, a model is established to analyze the additional stresses in the floor strata induced by mining activities. And some distribution features of all the additional stress components are described. By using the superposition principle in fracture mechanics, another model is developed to analyze the crack growth in the floor strata under the action of disturbed stresses and water pressure. And the stress intensity factors at the crack tip are presented and the process of crack growth is obtained in the advancement of a working face. Because of discretizing only loading areas and crack surfaces, the present methods can obtain the accurate numerical results. Finally, some suggestions are made for preventing the water inrush from a confined aquifer.

1. Introduction

In the coalfields of North China, coal seams are underlain by Ordovician limestone, which is strongly karstified and highly permeable. In most cases, the limestone aquifer contains an abundant supply of water and is confined. The activities of mining these coal seams are threatened with the confined water from the Ordovician limestone. Water inrush accidents result in heavy losses and casualties [1, 2]. With coal mining being executed in deeper sites, the pressure of confined water becomes larger and this type of water inrushes may occur more frequently.

In order to avoid water inrushes and keep the mines safe, large-scale dewatering or depressurizing of the Ordovician aquifer was chosen. In practice, dewatering causes serious environmental problems such as surface subsidence and underground water pollution and reduces the amount of water available for supply in the area. To solve this dilemma, some researches were devoted to make full use of the uncontaminated karst water obtained from dewatering for water supply [3]. Another measure to prevent water inrushes is to use the floor strata between the coal seam and the aquifer as a protective rock pillar. However, once the strength of the floor strata is difficult to resist the invasion of high-pressure water, the confined water floods into working faces. In some cases, grouting into the rock layers is used to improve the strength of floor strata to resist the invasion of confined water. By taking these measures, the water in the Ordovician limestone can be preserved to some extent and the coal seams can be extracted in a relatively safe environment.

As early as in 1979, the field investigations of the floor strata were executed in Fengfeng coalfield, China, where mining activities were threatened by confined aquifers [4]. After that, more field investigations of floor strata were performed in different types of mines. In Jingxing coalfield, China, it was found that the joints in floor strata were impermeable before mining, and confined water passed through the joints and flooded into the mines after mining [5]. This phenomenon may be explained by the joint growth induced by mining activities and water pressure from a confined aquifer. Additionally, the test of water injection in boreholes was used for understanding the permeability variations in floor strata induced by mining activities [6, 7]. These measured data were further used to determine the failure zones directly below the coal seam and above the confined aquifer.

In the past several decades, other types of analytical methods have been employed to study mining with water pressure for preventing water inrushes. Wang et al. [8] established both physical and numerical models to gain a better understanding into fracture initiation and propagation in floor strata during a mining process. Yang et al. [9] and Li et al. [10] used finite element methods to understand the mechanisms of water inrushes. Because different coal seams have different vulnerabilities for water inrushes, Wu et al. [11] assessed the differences in vulnerability between multiple coal seams. To evaluate a major water inflow hazard in a mine, Rafiqul et al. [12] used boundary element methods to model the mining-induced stress field. Zuo et al. [13] explored the spatial morphology of karst collapse and employed the discontinuous deformation analysis method to investigate karst collapse.

Although a great deal of field investigations and numerical analyses have been performed and some research results of water inrushes have been obtained, all the mechanisms of water inrushes are not known and the water inrushes are often reported. It is estimated that more than 80 percent of water inrushes may occur in the case of the floor rocks having faults or joints. This means that faults and joints in floor strata may induce water inrushes under the action of water pressure from aquifers and mining activities. Therefore, the water inrushes induced by faults or joints in longwall mining need to be further studied.

The principal objectives of this paper are to understand the stress fields in floor strata induced by coal mining and to predict the joint growths in the floor strata of the coal seam threatened by confined water in the advancement of a working face. From now on, the term crack will be used to describe a joint. In this paper, firstly, two numerical methods to be used are briefly introduced. Secondly, a mechanical model for simulating coal mining is established and the additional stress fields induced by coal mining are presented. Thirdly, another mechanical model is established for analyzing the crack problems under the action of water pressure and mining activities, and the stress intensity factors (SIFs) are obtained for the cracks at different positions of floor strata. Finally, the crack growths are predicted using SIF values and fracture criteria, and some suggestions are made for preventing the water inrushes into working faces from confined aquifers in floor strata.

2. Analytical Methods for Elastic Fields and Crack Problems in a Layered Medium

2.1. Yue's Solution Based Numerical Method for Elastic Fields in a Layered Medium. Xiao et al. [14] developed a numerical method for assessing the elastic fields in an arbitrarily depth-heterogeneous medium subject to complex loads using Yue's solution. Yue's solution [15] is a fundamental singular solution for the generalized Kelvin problems of a multilayered elastic solid of infinite extent subject to concentrated point body vectors. The stresses and displacements at any points of a layered medium are described as

$$\sigma_{ij}(Q) = \int_S \sigma^*_{ijk}(Q,P)\, t_k(P)\, dS(P), \quad i,j,k = x,y,z \tag{1a}$$

$$u_i(Q) = \int_S u^*_{ik}(Q,P)\, t_k(P)\, dS(P), \quad i,k = x,y,z \tag{1b}$$

where $\sigma^*_{ijk}(Q,P)$ and $u^*_{ik}(Q,P)$ are, respectively, stresses and displacements of Yue's solution for the field point Q due to the unit force along the k direction at the source point P; $t_k(P)$ is the traction at the source point P; the integral domain S is the loading area. It should be noted that the subscript k is a dummy index.

The corresponding computer program LayerSmart3D was written in FORTRAN. The techniques adopted in LayerSmart3D primarily involve the discretization of the loading area into a finite number of quadrilateral elements. Values of the loads are inputted at the node points of the discretized area. Numerical verification of LayerSmart3D indicates that numerical solutions of high accuracy can be efficiently calculated for elastic fields induced by the distributed loads in a layered medium.

2.2. Yue's Solution Based DDM for Analyzing Crack Problems in a Layered Medium. Xiao and Yue [16, 17] developed a new displacement discontinuity method (DDM) for the analysis of crack problems in a layered medium of infinite extent. This approach is also based on Yue's solution [15] and the corresponding computer program LayerDDM3D was written in FORTRAN.

Assume that the crack surfaces consist of Γ^+ and Γ^-. In the global coordinates (x,y,z), the discontinuous displacements of the crack surfaces are defined as $\Delta u_j(Q_{\Gamma^+}) = u_j(Q_{\Gamma^+}) - u_j(Q_{\Gamma^-})$. u_j is a displacement along the direction $j = x,y,z$. The traction on the crack surface is defined as $t_j(P_{\Gamma^+})$. The basic equations of Yue's solution based DDM are as follows:

$$t_j(P_{\Gamma^+}) + n_i(P_{\Gamma^+}) \int_{\Gamma^+} T^*_{ijk}(P_{\Gamma^+},Q)\, \Delta u_k(Q)\, d\Gamma(Q) = 0, \qquad i,j,k = x,y,z \tag{2}$$

where $n_i(P_{\Gamma^+})$ is the unit outward normal of the positive side of the crack surface at the source point P_{Γ^+} and $T^*_{ijk}(P_{\Gamma^+},Q)$ is a new kernel function which can be calculated by using the traction t^*_{ij} of Yue's solution.

In developing the DDM for (2), the nine-node continuous and discontinuous elements are used to discretize a crack surface. Kutt's numerical method is used to calculate the hypersingular integral in the integral equation. By solving the discretized equations of (2), the discontinuous displacements on the crack surface can be obtained. The numerical verification shows that the present results are in very good agreement with the existing ones. However, the proposed DDM is only suitable for the analysis of crack problems in layered media of infinite extent under the action of loadings on crack surfaces. Other types of crack problems in infinite media can be analyzed by using the two numerical methods together.

Table 1: The roof and floor strata of the extracted coal seam in No. 2710 working face.

Strata	Thickness(m)	Elastic modulus (GPa)	Poisson's ratio
Sandstone	14	25	0.28
Extracted coal seam	1.5	4	0.33
Sandstone	17	25	0.28
Limestone	5	40	0.28
Shale	4.2	15	0.29
Coal seam	1.8	4	0.33
Shale	20	20	0.30
Ordovician Limestone	Larger than 650	45	0.30

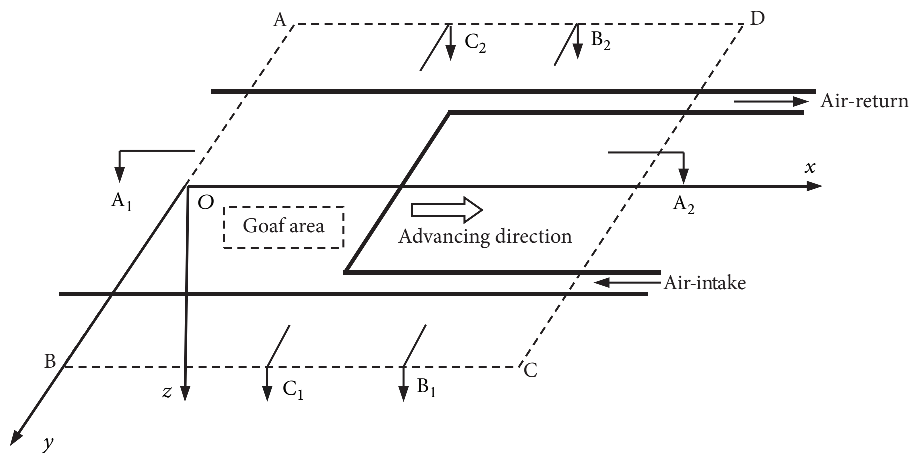

Figure 1: The disturbed area ABCD induced by coal mining.

2.3. The Analytical Methods of Crack Problems in Layered Media. In the following, the two numerical methods mentioned above, i.e., LayerSmart3D and LayerDDM3D, and the superposition principle in fracture mechanics are utilized to analyze crack problems in a layered medium. LayerSmart3D is firstly employed to obtain the stress fields of a layered medium without a crack under the action of distributed loadings within layered media. Using the superposition principle [18], the tractions, whose values are equal to the mining-induced stress and which have opposite directions, are then applied on the crack surfaces in the layered medium without the above distributed loadings. LayerDDM3D is finally employed to obtain the discontinuous displacements of the crack surfaces under the action of the above tractions. The SIF values at the crack tip can be calculated by using the discontinuous displacements of the crack surfaces and the relationship between SIFs and discontinuous displacements.

3. The Additional Stresses of Floor Strata without Cracks Induced by Mining

3.1. Geological and Mining Conditions of the Working Face. Jing et al. [4] investigated the deformation and failure of floor strata in mining the coal seam threatened by confined water in No. 2 Coal Mine of Fengfeng coalfield. No. 2710 working face in this mine was chosen for field measurements. Table 1 describes the roof and floor strata of the extracted coal seam. The coal seam is about 48 m away from the Ordovician limestone in which the water pressure ranges from 1.5 to 2 MPa. The working face is located at a depth of about 145 m and the longwall panel is 90 m long and 350 m wide. The coal seam is 1.5 m thick and the dip angle is about 1-3°. For the sake of simplicity, the rock strata are treated as horizontal media in developing a mechanical model. The working face was advanced along the strike direction of the coal seam. From August 1979 to February 1980, comprehensive measurements of floor deformation and failure were performed in the advancing process of the working face. In the field measurements, large amounts of data were obtained and will be further employed to analyze the water inrush from confined aquifers here.

3.2. A Model of Analyzing Additional Stresses of Floor Strata Induced by Mining

3.2.1. The Mining-Disturbed Area on the Interface of Coal Seam and Floor. Figure 1 illustrates the disturbed area ABCD on the interface between the mined coal seam and the floor. It is assumed that the domain out of the area ABCD is not disturbed by coal mining. According to the in situ investigations, the disturbed area ABCD is 150 m long and

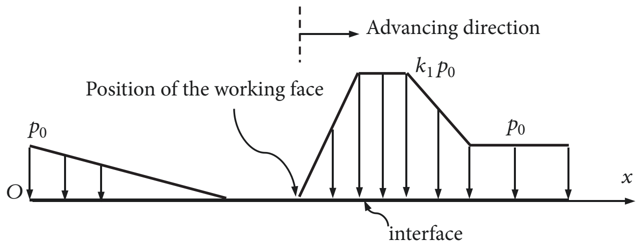

(a) Vertical stress on the interface of coal seam and floor for the disturbed case

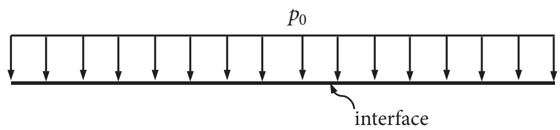

(b) Vertical stress on the interface of coal seam and floor for the undisturbed case

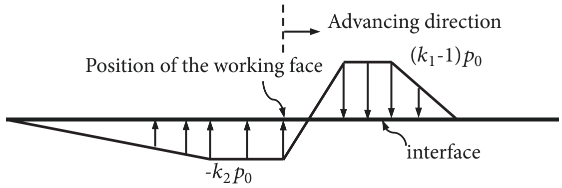

(c) Additional vertical stress on the interface of coal seam and floor for the disturbed case

Figure 2: Analytical method of additional vertical stress on the interface of coal seam and floor along the cross section A_1-A_2.

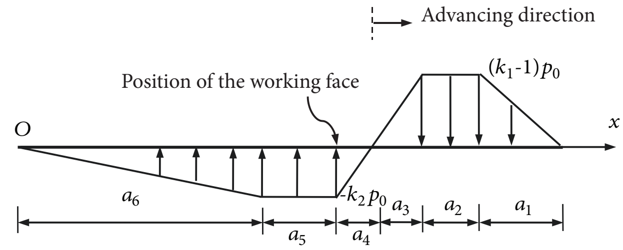

(a) Additional vertical stress on the interface of coal seam and floor along the cross section A_1-A_2

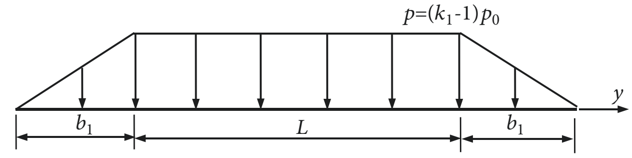

(b) Additional vertical stress on the interface of coal seam and floor along the cross section B_1-B_2

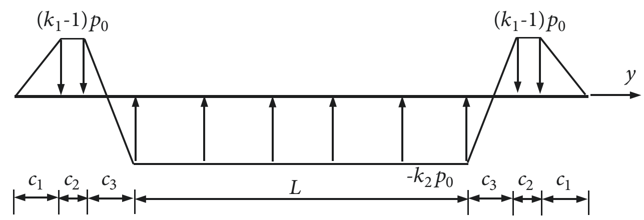

(c) Additional vertical stress on the interface of coal seam and floor along the cross section C_1-C_2

Figure 3: Additional vertical stress on the interface of coal seam and floor along different cross sections.

150 m wide. The vertical stress on the interface of the coal seam and the floor strata, which are not disturbed by mining, can be calculated using the following formula:

$$p_0 = \gamma h = 25 \times 145 = 3625 kN/m^2 \tag{3}$$

where γ is the average unit weight of the overlying strata and h is the depth of the extracted coal seam below the ground surface.

Mining activities induce the stress concentration on the coal pillars and floor around the working face. In the field investigations at No. 2710 working face, the disturbed area and stress concentration on the coal seams were obtained. Based on these data, we develop a model for the analysis of the influence of coal mining on floor strata.

The vertical stresses along different cross sections on the disturbed area are assumed by using the measured data. The concentration factors of the vertical stress ahead of and behind the working face along the cross section A_1-A_2 are taken to be $k_1 = 3$ and $k_2 = 1$, respectively. And the stress concentration factors along the cross sections B_1-B_2 and C_1-C_2 are taken to be $k_1 = 3$. On the floor strata near the roadways and the working face, the stresses are highly concentrated and the stress concentration factor is taken to be $k_3 = 3.5$. The stress concentration factors along other cross sections can be obtained by using the methods of linear or quadratic interpolation.

Figure 2 illustrates the process of obtaining the additional vertical stress on the interface of coal seam and floor along the cross section A1-A2 shown in Figure 1. It can be found that the additional vertical stress in Figure 2(c) is obtained by subtracting out the weight p_0 of the overburden above the mined coal seam in Figure 2(b) from the vertical pressure in Figure 2(a). Figure 3 presents the additional vertical stresses on the interface between coal seam and floor along three different cross sections. Based on the data from in situ measurements, the parameters of lengths shown in Figure 3(a) are presented as follows: $a_1 = 40$m, $a_2 = 10$m, $a_3 = 5$m, $a_4 = 5$m, $a_5 = 30$m, and $a_6 = 60$m. The parameters of lengths shown in Figure 3(b) are presented as follows: $L = 90$m and $b_1 = 30$m. The parameters of lengths shown in Figure 3(c) are presented as follows: $L = 90$m, $c_1 = 30$m, $c_2 = 30$m, and $c_3 = 30$m.

3.2.2. Element Mesh of the Disturbed Area and Comparison of Numerical and Field Results. In order to analyze the elastic fields using the software LayerSmart3D, the disturbed area ABCD is discretized into the mesh with 2610 nodes and 8037 elements, shown in Figure 4. The additional vertical stresses on the disturbed area ABCD (see Figure 3) are applied on the nodes of the element mesh. Figure 5 illustrates the distribution of the additional vertical stress on the interface of coal seam and floor. It can be found that the distribution of the additional vertical stress shown in Figure 5 is in good agreement with the one shown in Figure 3.

After presenting the mechanical parameters of floor strata in Table 1 and the additional vertical stress in Figure 5, the

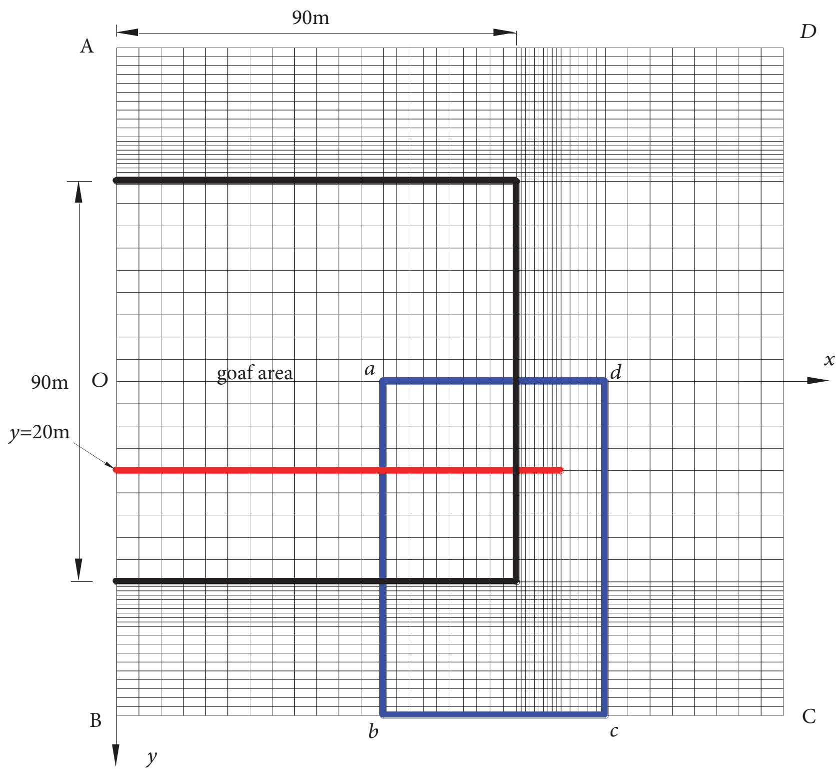

Figure 4: Element mesh of the disturbed area ABCD, the projection *abcd* of the calculating area at $z = 15$m, and the plane at $y = 20$m for calculating the stresses.

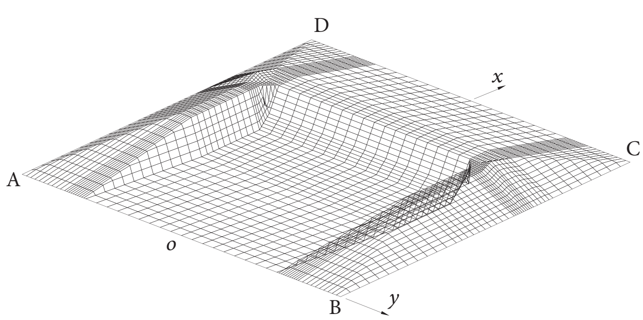

Figure 5: Additional vertical stress on the disturbed area ABCD.

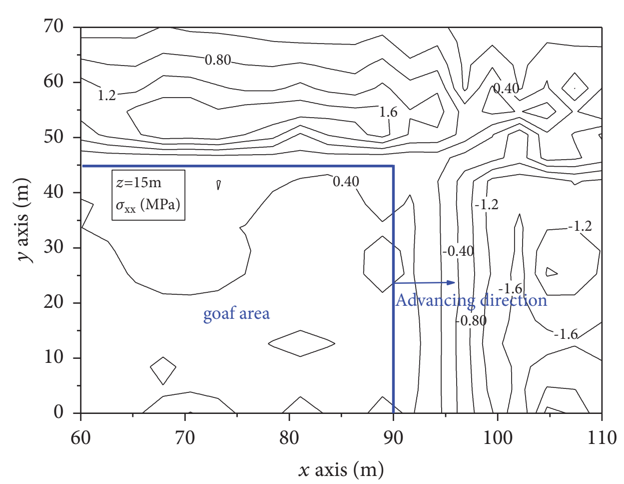

Figure 6: Contours of the additional stress σ_{xx} at the depth $z = 15$m.

software LayerSmart3D is used to obtain the stress and displacement fields of floor strata. Table 2 lists the vertical displacements at some points in the floor strata from numerical analyses and in situ measurements. It can be found that the displacements from the two methods are much close to each other if the differences of the geological and mining conditions for two methods are considered.

3.3. Variations of Additional Stresses in Floor Strata Induced by Mining

3.3.1. Distribution of Additional Stresses at the Depth $z = 15$m. As shown in Figure 4, the model is symmetric with respect to the coordinate plane *Oxz*. Thus, the rectangular area, i.e., $60\,\text{m} \le x \le 110$m, $0\,\text{m} \le y \le 45$m, and $z = 15$m, is chosen to calculate the additional stresses. This area has a projection *abcd* on the coordinate plane *Oxy* shown in Figure 4. Figures 6–11 illustrate the distribution of all the stress components on the calculating area.

Figures 6–8 show the variations of three normal stresses in the floor strata. In Figure 6, the rectangular area can be divided into three areas by considering the distribution features of σ_{xx}. Below the goaf area, σ_{xx} is tensile and has small values. Below the coal seam in the front of the working face,

Table 2: Comparison of maximum vertical displacements from in situ measurements and numerical analyses along the advancing direction (unit: mm).

Positions (y, z)	ahead of the face wall		behind the face wall	
	In situ measurements	This study	In situ measurements	This study
$(0, 4.9)$	8	9.9995	5	-2.7071
$(0, 6.2)$	8	9.7000	-2	-2.5608
$(0, 10.2)$	7	8.9472	1	-2.1707
$(40, 2.4)$	13	10.3224	6	8.9056
$(40, 4.7)$	14	9.3394	13	7.0610
$(40, 7.2)$	14	9.6763	16	8.2905

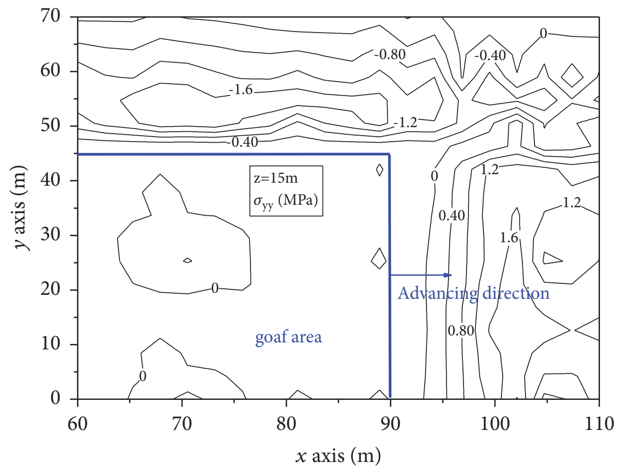

Figure 7: Contours of the additional stress σ_{yy} at the depth $z = 15$m.

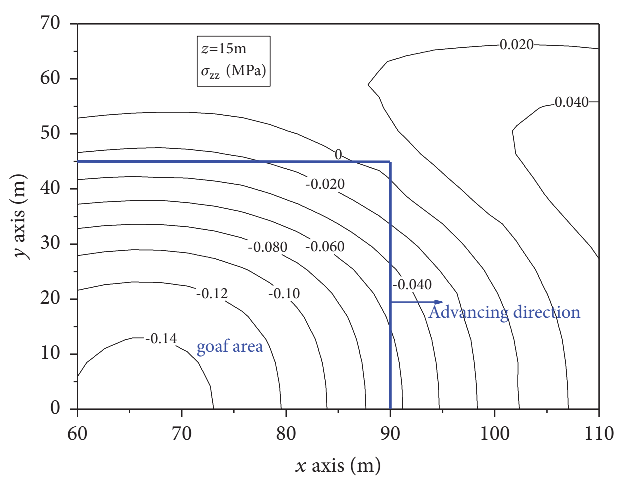

Figure 8: Contours of the additional stress σ_{zz} at the depth $z = 15$m.

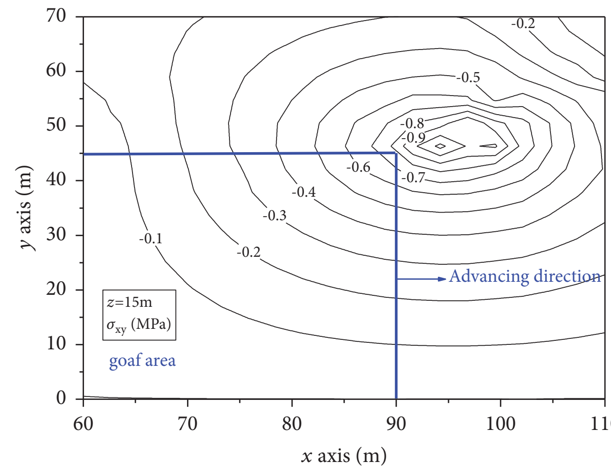

Figure 9: Contours of the additional stress σ_{xy} at the depth $z = 15$m.

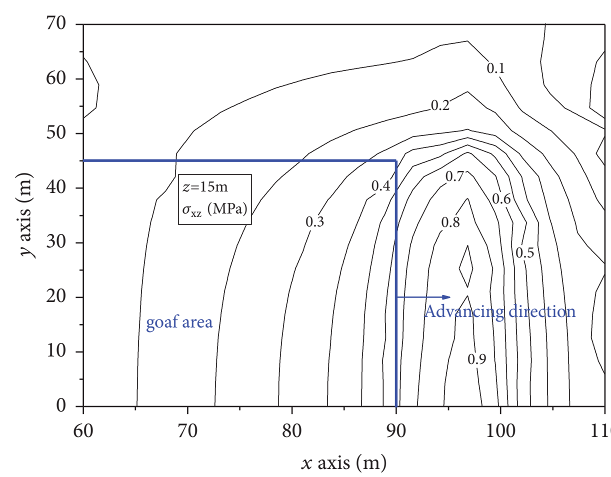

Figure 10: Contours of the additional stress σ_{xz} at the depth $z = 15$m.

σ_{xx} is compressive and its minimum value is about -1.6 MPa. And below the coal pillar outside the goaf area, σ_{xx} is tensile and its maximum value is about 1.6 MPa. In Figure 7, the rectangular area can also be divided into three areas. Below the goaf area, σ_{yy} approaches zero. Below the coal seam in the front of the working face, σ_{yy} is tensile and its minimum value is about 1.6 MPa. And below the coal pillar outside the goaf area, σ_{yy} is compressive and its minimum value is about 1.6 MPa. In Figure 8, the rectangular area can be divided into two areas. σ_{zz} is compressive below the goaf area and is tensile away from the goaf area.

Figures 9–11 show the variations of three shear stresses in the floor strata. In Figure 9, σ_{xy} has a maximum value of

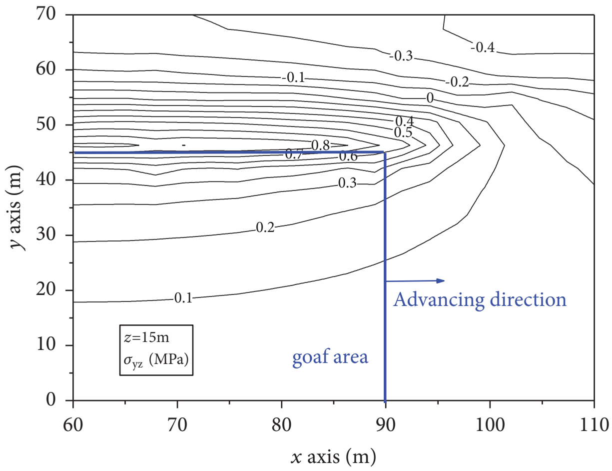

Figure 11: Contours of the additional stress σ_{yz} at the depth z = 15m.

about -1.0 MPa at the point $(x, y, z) = (94\text{m}, 46\text{m}, 15\text{m})$ and σ_{xy} becomes small away from this point. In Figure 10, σ_{xz} is concentrated in the front of the working face and becomes small away from this zone and its maximum value is about 1.0 MPa. In Figure 11, σ_{yz} is concentrated below the coal pillar outside the goaf area and becomes small away from this zone.

3.3.2. Distribution of the Additional Stresses in the Plane y = 20m. Figures 12–17 illustrate the distribution of all the stress components in the plane $y = 20\text{m}$ for different x and z values. As shown in Figure 4, this plane is along the advancing direction of the working face and has a horizontal distance of 25 m from the coal pillar outside the goaf. For the sake of simplification, the stress variations are referred to as the ones with the depth increasing in the following analyses. From these figures, we can have the following observations:

(i) At $x = 0\text{m}$, all the stresses have very small values because the position is away from the maximum loadings. In the first and second layers, the stresses vary obviously with depth. In the other layers, all the stresses are very small and vary weakly with depth.

(ii) σ_{xx} has small values in the first layer and the absolute values of σ_{xx} increase in the second layer. In the first layer, σ_{yy} increases at $x = 100\text{m}$ whilst σ_{yy} decreases at the other x values. In the second layer, σ_{yy} is negative and decreases. At $x = 40, 81\text{m}$, σ_{zz} is positive and decreases. At $x = 90\text{m}$, σ_{zz} is positive in the first layer and negative in the other remaining layers and decreases. σ_{zz} is negative and decreases at $x = 95\text{m}$, and σ_{zz} is negative and increases at $x = 100\text{m}$.

(iii) At $x = 0, 40\text{m}$, σ_{xy} decreases in the first, second, and third layers and increases in the remaining two layers. The variation of σ_{xy} at $x = 81, 90, 95, 100\text{m}$ is different from the one at $x = 0, 40\text{m}$. σ_{xz} is negative at $x = 0, 40\text{m}$ whilst σ_{xz} is positive at $x = 81, 90, 95, 100\text{m}$. In the different layers, σ_{xz} first increases and then decreases for a given z value from $x = 81$ to 100 m. The absolute values of σ_{xz} first increase and then decrease. σ_{yz} is always positive for all the x values. For $x = 0\text{m}$, σ_{yz} increases. Except for $x = 0\text{m}$, in the first

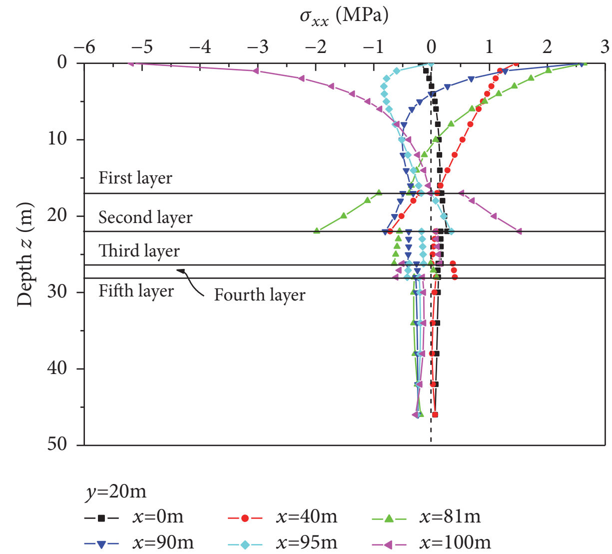

Figure 12: Variations of the additional stress σ_{xx} with depth at y = 20m.

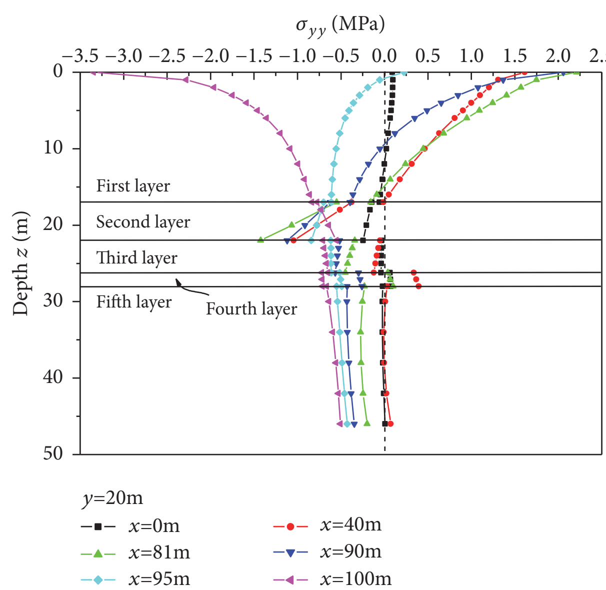

Figure 13: Variations of the additional stress σ_{yy} with depth at y = 20m.

and second layers, σ_{yz} first increases and then decreases. And from the third layer to the fifth layer, σ_{yz} first increases and then decreases.

4. A Model of Analyzing Crack Problems in Floor Strata

As shown in Figure 18, a rectangular crack is located in floor strata and is subject to mining-disturbed stresses and water pressure. A global coordinate system $Oxyz$, which is completely the same as the one shown in Figure 1, is attached to the model to be analyzed and a local coordinate system $O'x'y'z'$ is attached on the crack surface. The rectangular crack is 2 m

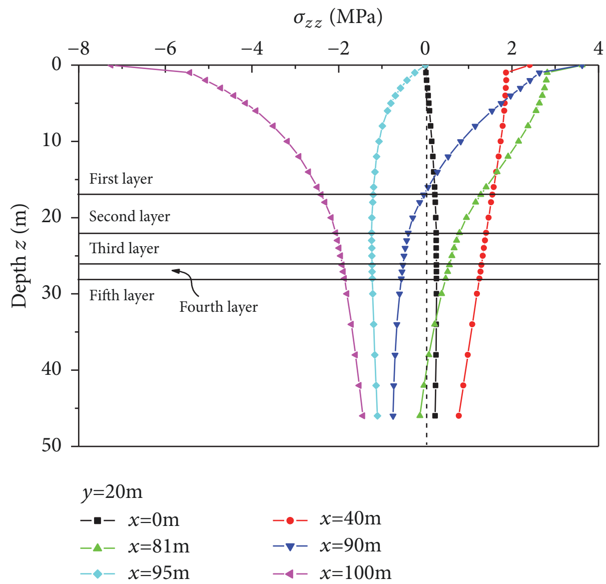

FIGURE 14: Variations of the additional stress σ_{zz} with depth at y = 20m.

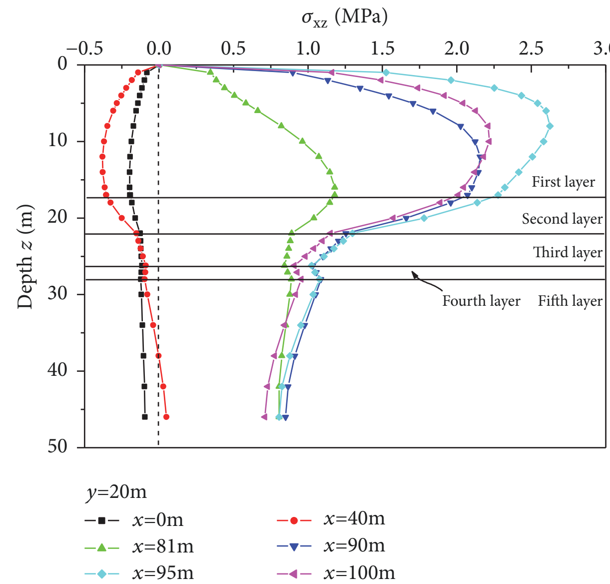

FIGURE 16: Variations of the additional stress σ_{xz} with depth at y = 20m.

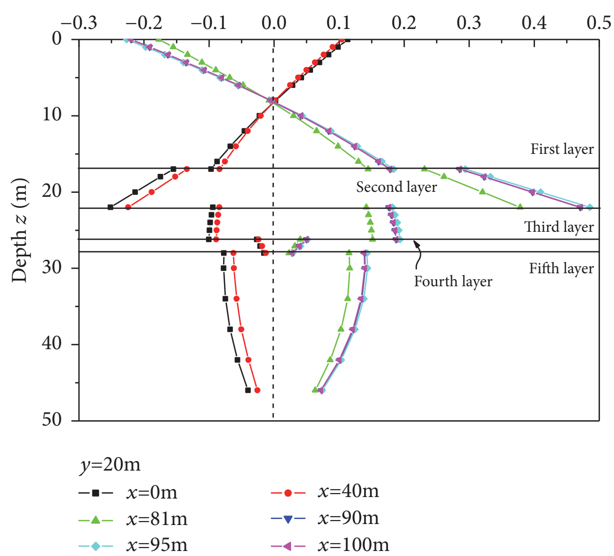

FIGURE 15: Variations of the additional stress σ_{xy} with depth at y = 20m.

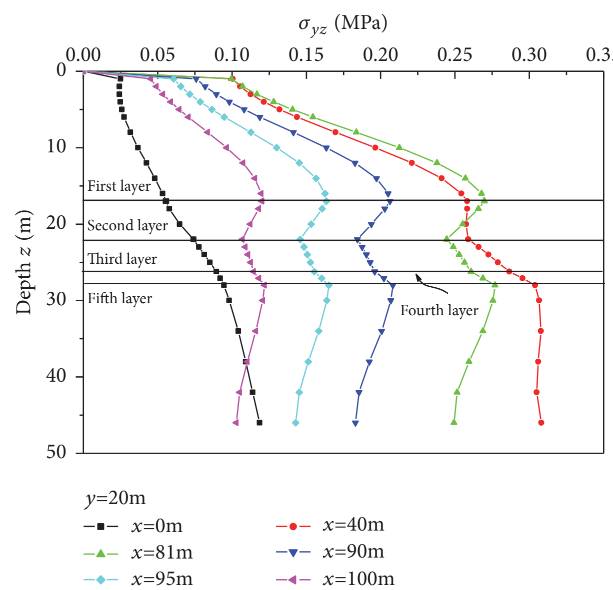

FIGURE 17: Variations of the additional stress σ_{yz} with depth at y = 20m.

wide (AB and CD sides) and 4 m long (AD and BC sides). Assume that the crack surfaces are parallel to the advancing direction of the working face and the crack center is located at the point $(x, y, z) = (d_1, d_2, 46\text{m})$.

Using the superposition principle in fracture mechanics [18], the disturbed stresses induced by mining activities can be transformed to the tractions on the crack surfaces. The disturbed stresses should be the summation of the horizontal normal stress σ_h induced by rock weights and the additional stresses $(\sigma_{yy}, \sigma_{xy}, \sigma_{zy})$ induced by mining activities. Additionally, the crack surfaces are subject to the water pressure p_w from confined aquifer. Thus, the crack surfaces are subjected to the following tractions:

$$f_x = -\sigma_{xy} \tag{4a}$$

$$f_y = -\left(\sigma_{yy} + \sigma_h\right) + p_w \tag{4b}$$

$$f_z = -\sigma_{yz} \tag{4c}$$

where p_w is taken to be 2 MPa.

In (4b), σ_h is calculated by the following formula:

$$\sigma_h = \frac{\nu}{1-\nu}\gamma h \tag{5}$$

where ν and γ are, respectively, the average values of Poisson's ratio and unit weight of rock strata and h is the depth of the

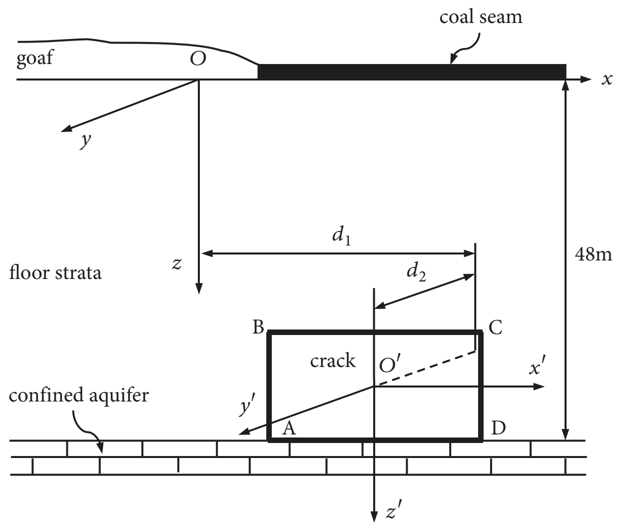

FIGURE 18: Model of analyzing crack problems in floor strata under the action of distributed stresses and water pressure.

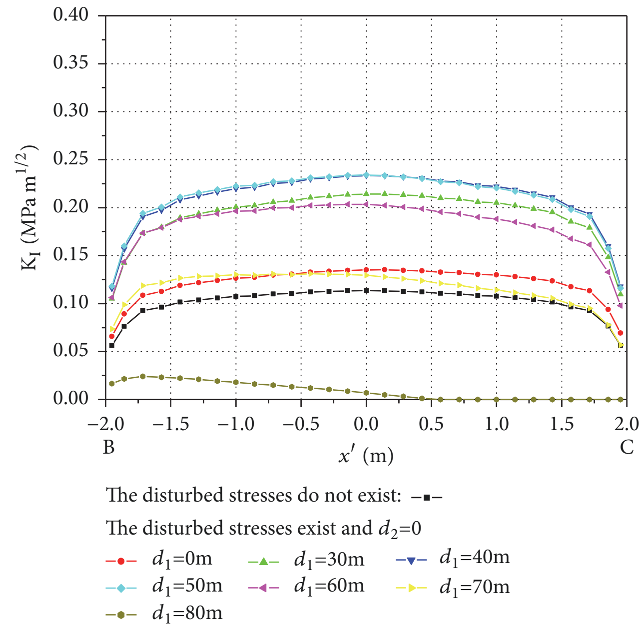

FIGURE 19: Variations of K_I values at the crack side (BC) for Case 1.

crack center below the ground surface. Take $\gamma = 25\text{kN/m}^2$, $\nu = 0.28$, and $h = 192\text{m}$. Thus, $\sigma_h \approx 1.8667\text{MPa}$.

The crack surface is discretized into 435 nodes and 98 nine-node elements with 60 nine-node isoparametric elements, 34 discontinuous elements of type I, and four discontinuous elements of type II. The discontinuous displacements of the crack surfaces can be obtained using the element mesh, the tractions (f_x, f_y, f_z) on the crack surface, and the computer code LayerDDM3D.

5. SIFs of Cracks under the Action of Water Pressure and Disturbed Stresses

5.1. General. The stress intensity factors (SIF) values at the crack tip can be calculated by using the discontinuous displacements of crack surfaces. When the crack is not located at the interfaces of multilayered solids, the crack tip field singularities and angular distributions are the same as those in a homogeneous medium and the material parameters exert an influence on the magnitudes of the SIFs. Based on the relationship of displacements and the SIFs, the formulae of the SIFs along the crack side BC are as follows:

$$K_{\mathrm{I}} = \frac{E}{4(1-\nu^2)}\sqrt{\frac{\pi}{2r}}\Delta u_{y'} \quad (r, \theta = \pm\pi, \varphi = 0), \tag{6a}$$

$$K_{\mathrm{II}} = \frac{E}{4(1-\nu^2)}\sqrt{\frac{\pi}{2r}}\Delta u_{z'} \quad (r, \theta = \pm\pi, \varphi = 0), \tag{6b}$$

$$K_{\mathrm{III}} = \frac{E}{4(1+\nu)}\sqrt{\frac{\pi}{2r}}\Delta u_{x'} \quad (r, \theta = \pm\pi, \varphi = 0), \tag{6c}$$

where (r, θ, φ) is the spherical coordinates located at the crack front and θ is an angle in the coordinate plane normal to the crack line of crack front.

The following two cases are analyzed: Case 1: a rectangular crack is located in the coordinate plane Oxz, i.e., $d_2 = 0\text{m}$; Case 2: a rectangular crack is located in the plane $y = 40\text{m}$, i.e., $d_2 = 40\text{m}$.

5.2. Case 1: The Crack Is Located in the Coordinate Plane Oxz. In this case, the shear stresses σ_{xy} and σ_{zy} in the coordinate plane Oxz are equal to zero because of the symmetry of the model. As a result, K_{II} and K_{III} are equal to zero. Figure 19 illustrates the variations of K_{I} for the crack at different positions along the advancing direction of the working face. For the crack only subject to water pressure, the maximum value of K_{I} is $0.1134\,\text{MPa}\cdot\text{m}^{1/2}$. However, for the crack subject to water pressure and disturbed stresses, the maximum value of K_{I} is $0.1351\,\text{MPa}\cdot\text{m}^{1/2}$ at $d_1 = 0\text{m}$. With d_1 increasing, K_{I} increases, arrives at maximum values at $d_1 = 40, 50\text{m}$, and then decreases. For $d_1 = 80\text{m}$ and $x' \geq 0.5\text{m}$, K_{I} is equal to zero and K_{I} along the whole BC side is equal to zero at $d_1 \geq 90\text{m}$. These findings mean that the crack below the coal seam is closed and the crack below the goaf is opened under the action of disturbed stresses and water pressure. When the crack is located at some horizontal distance of 40-50m after the coal wall of the working face, there are the maximum opening displacements. In this case, the crack becomes easy to open and induces the uplifting of the confined water.

5.3. Case 2: The Crack Is Located in the Plane $y = 40\text{m}$, i.e., $d_2 = 40\text{m}$. In this case, the crack is close to the coal pillars outside the working face and has a horizontal distance of 5 m from the coal pillar. As discussed in Section 3, the shear stresses induced by mining exist at this position and as a result the crack has three types of fracture modes. Figures 20–22 show the variations of K_{I}, K_{II}, and K_{III} along the crack front BC, respectively.

In Figure 20, the K_{I} values for $d_1 = 0, 40\text{m}$ are very close to the ones of the crack only subject to water pressure whilst

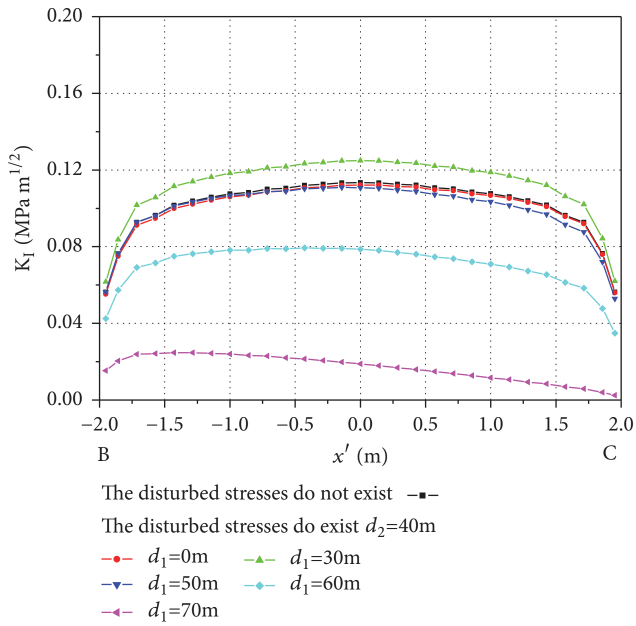

FIGURE 20: Variations of K_I values at the crack side (BC) for Case 2.

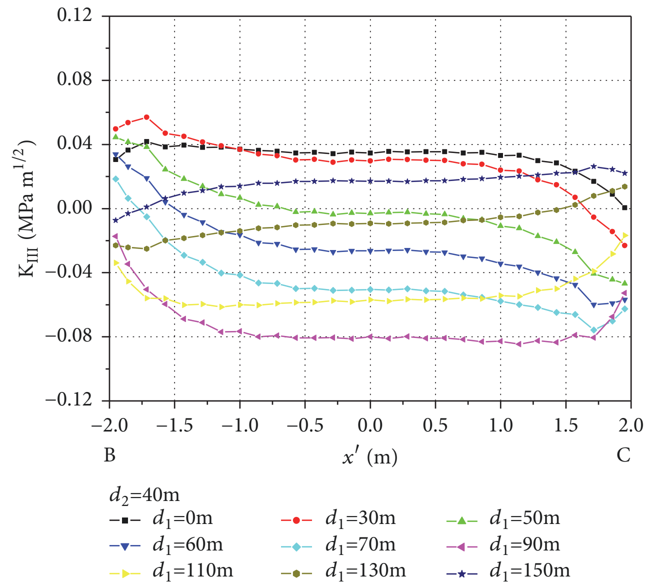

FIGURE 22: Variations of K_{III} values at the crack side (BC) for Case 2.

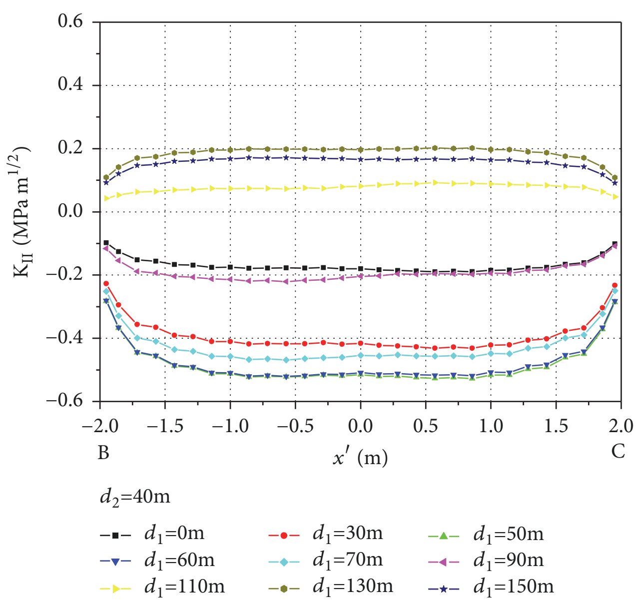

FIGURE 21: Variations of K_{II} values at the crack side (BC) for Case 2.

the K_I values for $d_1 = 30$m are larger than the ones of the crack only subject to water pressure. As the d_1 values increase ($d_1 \geq 30$m), the K_I values decrease. When $d_1 \geq 90$m, the K_I values are equal to zero. This means that the crack directly below the goaf is opened and the crack directly below the coal seam is closed under the action of water pressure and disturbed stresses. By comparing the values shown in Figures 19 and 20, it can be found that the K_I values for $d_2 = 40$m are smaller than the ones for $d_2 = 0$m at a given d_1 value.

In Figure 21, the K_{II} values are, respectively, negative and positive for $d_1 = 0 - 90$m and $d_1 = 110 - 150$m. For $d_1 = 0-90$m, as the d_1 values increase, the K_{II} values first decrease, arrive at the minimum values at $d_1 = 50$m, and then increase. For $d_1 = 110 - 150$m, as the d_1 values increase, the K_{II} values first increase, arrive at the maximum values at $d_1 = 130$m, and then decrease. It is believed that the K_{II} values tend to zero when the absolute values of d_1 tend to an infinite value.

In Figure 22, the K_{III} values for $d_1 = 0$m are positive. As the d_1 values increase, the K_{III} values decrease along the most part of the crack side BC, become negative values, and arrive at the minimum values at $d_1 = 90$m. Then, the K_{III} values increase along the most part of the crack side BC. It is believed that the K_{III} values tend to zero when the absolute values of d_1 tend to an infinite value.

6. Analysis of Crack Growths Induced by Mining

6.1. Case 1: The Crack Is Located in the Coordinate Plane Oxz. As discussed in Section 5.2, the crack has only mode I deformation type in this case. The crack growth can be analyzed by using the fracture criterion $K_I = K_{IC}$. Chong et al. [19] investigated the fracture toughness K_{IC} of layered rocks by using three-point-bend specimens and presented the K_{IC} values of oil shale. Using an analogical method, the K_{IC} value of the shale in Table 1 is estimated to be $0.74\,\mathrm{MPa}\cdot\mathrm{m}^{1/2}$. As shown in Figure 19, the maximum K_{Imax} values are about $0.2335\,\mathrm{MPa}\cdot\mathrm{m}^{1/2}$ and $K_{Imax} < K_{IC}$. This means that this type of crack does not grow and the confined water does not uplift under the action of water pressure and disturbed stresses.

6.2. Case 2: The Crack Is Located in the Plane $y = 40$m, i.e., $d_2 = 40$m. As discussed in Section 5.3, the mode I, II, and III deformations of the crack are coupled together. Growth of a crack in elastic solids subject to complex stress states can be assessed using the so-called S-criterion proposed by

Sih [20]. The S-criterion was developed on the basis of the strain energy density concept. It states that local instability is assumed to occur when the local minimum energy factor S_{min} reaches a critical value S_{cr}. Using the fracture criterion and the SIF values in Section 5.3, the crack growth for Case 2 will be discussed in the following.

The strain energy density factor S of a three-dimensional crack can be defined as [21]

$$S(\theta) = a_{11}(\theta) K_{\mathrm{I}}^2 + 2a_{12} K_{\mathrm{I}} K_{\mathrm{II}} + a_{22}(\theta) K_{\mathrm{II}}^2 + a_{33}(\theta) K_{\mathrm{III}}^2 \tag{7}$$

where

$$\begin{aligned} a_{11}(\theta) &= \frac{1}{16\pi\pi\mu}(3 - 4\mu - \cos\theta)(1 + \cos\theta) \\ a_{12}(\theta) &= \frac{1}{8\pi\mu}\sin\theta(\cos\theta - 1 + 2\nu) \\ a_{22}(\theta) &= \frac{1}{16\pi\mu}[4(1-\nu)(1-\cos\theta) \\ &\quad + (3\cos\theta - 1)(1 + \cos\theta)] \\ a_{33} &= \frac{1}{4\pi\mu} \end{aligned} \tag{8}$$

where μ is the shear modulus of elasticity, ν is Poisson's ratio, and θ is an angle in the coordinate plane normal to the crack line of crack front.

Using the SIF values presented in Section 5.3 and (7), the local minimum energy factor S_{min} can be calculated. Figure 23 illustrates the variations of S_{min} values with the distance d_1. At $d_1 = 0, 90, 110, 130, 150$m, the S_{min} values are smaller than the ones at $d_1 = 30, 50, 60, 70$m. From $d_1 = 0$ to 90 m, S_{min} first increases, arrives at the maximum value at $d_1 = 50$m, and then decreases. From $d_1 = 90$ to 150 m, S_{min} first decreases, arrives at the minimum value at $d_1 = 110$m, and then increases. It can be estimated that S_{min} tends to zero as the floor strata are far from the coal wall of the working face.

The following conclusions can be drawn:

(i) For $d_1 \leq 90$m, S_{min} is the largest at $d_1 = 50$m whilst for $d_1 > 90$m, S_{min} is the largest at $d_1 = 110$m. This means that S_{min} has two largest values before and after the coal pillar of the working face. Whether the crack grows or not depends on the S_{cr} magnitude of the shale.

(ii) The maximum values of S_{min} at $d_1 = 50$m are larger than the ones at $d_1 = 110$m. The crack growth becomes easy when the crack is located below the goaf. It has been found that the K_{I} values for Case 1 are the largest at $d_1 = 40, 50$m. This means that the growth of any cracks parallel to the coordinate plane Oxz is easy at some horizontal distance of 40-50m behind the coal wall of the working face.

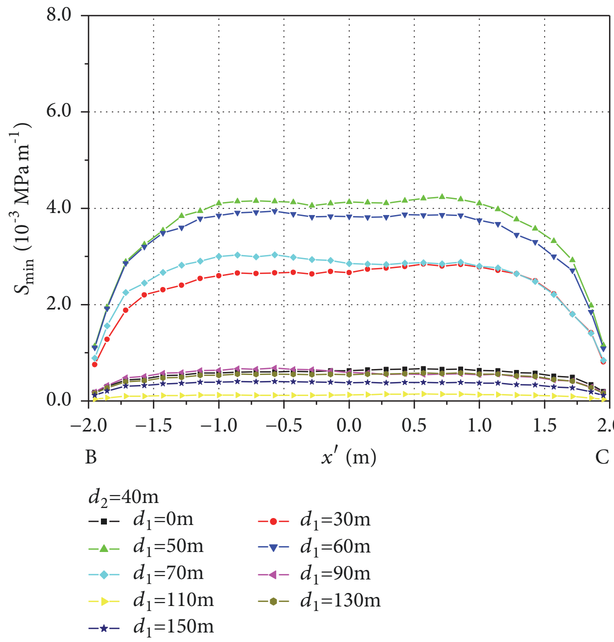

FIGURE 23: Variations of S_{min} values at the crack side (BC) for Case 2.

7. Conclusions

Numerical methods and mechanical models have been proposed for analyzing the stress fields and crack growths in floor strata for longwall mining. The additional stresses in the floor strata induced by mining are calculated and the crack problems subject to mining-induced stresses and water pressure are investigated. The research results presented in this paper can be summarized as follows:

(1) The additional stresses of the floor strata for longwall mining are described in detail and the distribution features of all the stress components with the depth below the floor and the distance from the working face are obtained.

(2) By analyzing the crack problems under the action of water pressure and disturbed stresses, the SIF values of the crack at different positions of floor strata are obtained. When the crack is located in the coordinate plane Oxz, only the mode I deformation of the crack exists. However, when the crack is not located in the coordinate plane Oxz, the mode I, II, and III deformations of the crack are coupled together.

(3) At some horizontal distance of 40-50m behind the working face, the vertical crack in the coordinate plane Oxz has the largest values of K_{I} and the vertical crack, which is not located in the coordinate plane Oxz, has the largest values of S_{min}. At these positions, the crack growths become easier. Therefore, the field measures should be taken in the advancement of the working face to prevent the water inrushes into the goaf behind working faces.

It is the authors' belief that the analytical methods presented in this paper can be a powerful numerical tool, which can apply to other types of cracks in the floor strata of the coal seam threatened by confined aquifers. Some of the related problems are currently under investigation by the authors for further understanding the complex mechanisms of water inrushes.

Data Availability

The [DATA TYPE] data used to support the findings of this study are included within the article.

Conflicts of Interest

The authors declare that they have no conflicts of interest.

Acknowledgments

The work presented in this paper was supported by the National Natural Science Foundation of China (Grant No. 41672291) and SDUST Research Fund (2015TD-JH104).

References

[1] W. F. Zhou, "Karst water control and management in the Hanxing mining are of North China," *Environmental Geology*, vol. 3-4, no. 30, pp. 280–284, 1997.

[2] G. Li and W. Zhou, "Impact of karst water on coal mining in North China," *Environmental Geology*, vol. 49, no. 3, pp. 449–457, 2006.

[3] Q. Wu, W. Zhou, D. Li, Z. Di, and Y. Miao, "Management of karst water resources in mining area: Dewatering in mines and demand for water supply in the Dongshan Mine of Taiyuan, Shanxi Province, North China," *Environmental Geology*, vol. 50, no. 8, pp. 1107–1117, 2006.

[4] Z. G. Jing, B. Y. Li, and Z. P. Sun, "In situ measurement of the floor strata failure in the No. 2 coal mine of Fengfeng coalfield," SDUST Project 1979-1, 1979 (Chinese).

[5] B. Y. Li, Z. P. Sun, and Z. C. Liu, "In situ measurement of the floor strata failure in the No. 3 coal mine of Jingxing coalfield," SDUST Project 1986-1, 1987.

[6] H. T. Xiao and H. Y. Xu, "In situ permeability measurements to establish the influence of slice mining on floor rocks," *International Journal of Rock Mechanics and Mining Sciences*, vol. 37, no. 5, pp. 855–860, 2000.

[7] J. Zhang, "Investigations of water inrushes from aquifers under coal seams," *International Journal of Rock Mechanics and Mining Sciences*, vol. 42, no. 3, pp. 350–360, 2005.

[8] J. A. Wang and H. D. Park, "Coal mining above a confined aquifer," *International Journal of Rock Mechanics and Mining Sciences*, vol. 40, no. 4, pp. 537–551, 2003.

[9] T. H. Yang, J. Liu, W. C. Zhu, D. Elsworth, L. G. Tham, and C. A. Tang, "A coupled flow-stress-damage model for groundwater outbursts from an underlying aquifer into mining excavations," *International Journal of Rock Mechanics and Mining Sciences*, vol. 44, no. 1, pp. 87–97, 2007.

[10] L. C. Li, T. H. Yang, Z. Z. Liang et al., "Numerical investigation of groundwater outbursts near faults in underground coal mines," *International Journal of Coal Geology*, vol. 85, no. 3-4, pp. 276–288, 2011.

[11] Q. Wu., Y. Z. Liu, and Y. Liu, "Using the Vulnerable Index Method to Assess the Likelihood of a Water Inrush through the Floor of a Multi-seam Coal Mine in China," *Mine Water and the Environment*, vol. 30, no. 1, pp. 54–60, 2011.

[12] M. R. Islam, D. Hayashi, and A. B. M. Kamruzzaman, "Finite element modeling of stress distributions and problems for multi-slice longwall mining in Bangladesh, with special reference to the Barapukuria coal mine," *International Journal of Coal Geology*, vol. 78, no. 2, pp. 91–109, 2009.

[13] J. P. Zuo, S. P. Peng, Y. J. Li, Z. H. Chen, and H. P. Xie, "Investigation of karst collapse based on 3-D seismic technique and DDA method at Xieqiao coal mine, China," *International Journal of Coal Geology*, vol. 78, no. 4, pp. 276–287, 2009.

[14] H. T. Xiao, Z. Q. Yue, and X. M. Zhao, "A generalized Kelvin solution based method for analyzing elastic fields in heterogeneous rocks due to reservior water impoundment," *Computers & Geosciences*, vol. 43, no. 6, pp. 126–136, 2012.

[15] Z. Q. Yue, "On generalized Kelvin solutions in a multilayered elastic medium," *Journal of Elasticity*, vol. 40, no. 1, pp. 1–43, 1995.

[16] H. T. Xiao and Z. Q. Yue, "A three-dimensional displacement discontinuity method for crack problems in layered rocks," *International Journal of Rock Mechanics and Mining Sciences*, vol. 48, no. 3, pp. 412–420, 2011.

[17] H. T. Xiao and Z. Q. Yue, *Fracture Mechanics in Layered And Graded Materials: Analysis Using Boundary Element Methods*, De Gruyter, Berlin, Germany, 2014.

[18] R. J. Sanford, *Principles of Fracture Mechanics*, Prentice Hall: Pearson Education, Inc., 2003.

[19] K. P. Chong, M. D. Kuruppu, and J. S. Kuszmaul, "Fracture toughness determination of layered materials," *Engineering Fracture Mechanics*, vol. 28, no. 1, pp. 43–54, 1987.

[20] G. C. Sih and B. C. K. Cha, "A fracture criterion for three-dimensional crack problems," *Engineering Fracture Mechanics*, vol. 6, no. 4, pp. 699–723, 1974.

[21] R. J. Hartranft and G. C. Sih, "Stress singularity for a crack with arbitrary curved front," *Engineering Fracture Mechanics*, vol. 9, no. 3, pp. 705–718, 1976.


Advances in
Operations Research
Advances in
Decision Sciences
Journal of
Applied Mathematics
The Scientific
World Journal
Journal of
Probability and Statistics
International
Journal of
Mathematics and
Mathematical
Sciences
Hindawi
Submit your manuscripts at
www.hindawi.com
Journal of
Optimization
International Journal of
Engineering
Mathematics
International Journal of
Analysis
Journal of
Complex Analysis
Advances in
Numerical Analysis
Mathematical Problems
in Engineering
International Journal of
Differential Equations
Discrete Dynamics in
Nature and Society
International Journal of
Stochastic Analysis
Journal of
Mathematics
Journal of
Function Spaces
Abstract and
Applied Analysis
Advances in
Mathematical Physics